Final Draft
of the original manuscript:

Ebel, T.; Blawert, C.; Willumeit, R.; Luthringer, B.J.C.; Ferri, O.M.; Feyerabend, F.:

Ti–6Al–4V–0.5B—A Modified Alloy for Implants Produced by Metal Injection Molding

In: Advanced Engineering Materials (2011) Wiley

DOI: 10.1002/adem.201180017

DOI: 10.1002/adbi.201100017

Ti-6Al-4V-0.5B – a modified alloy for implants produced by Metal Injection Moulding

By *Thomas Ebel, Carsten Blawert, Regine Willumeit, Bérengère J.C. Luthringer, Orley Milagres Ferri* and *Frank Feyerabend*

Dr. T. Ebel, Dr. C. Blawert, Prof. Dr. R. Willumeit, Dr. B.J.C. Luthringer, Dr. O.M. Ferri, Dr. F. Feyerabend
Institute of Materials Research, Helmholtz-Zentrum Geesthacht
Max-Planck-Straße 1, D-21502 Geesthacht, Germany
E-mail: thomas.ebel@hzg.de

Abstract

Permanent implants have to fulfil a great variety of requirements related to both material and geometry. In addition, manufacturing costs play a role, which is getting steadily more and more important. Metal Injection Moulding (MIM) of titanium alloy powders may contribute to the development of implants with higher functionality without increasing the price. High degree of freedom with regard to geometry, high material efficiency and the possibility to create even porous structures are main benefits from applying this technique. Today, even long-term implants made from Ti-6Al-4V by MIM are commercially available. However, in order to improve fatigue behaviour it is beneficial to perform a minor variation of Ti-6Al-4V by adding a low amount of boron. In this paper the mechanical, biological and corrosion properties of specimens manufactured from Ti-6Al-4V-0.5B alloy by MIM are presented. In order to exclude unknown reactions in the body environment due to the boron content, corrosion and biological tests are performed. Tensile and fatigue tests characterise the

mechanical properties. Potentiodynamic polarisation and electrochemical impedance spectroscopy are done in comparison to wrought and to MIM processed Ti-6Al-4V material. For cell experiments cancellous bone cells are cultured to perform adhesion, proliferation and viability experiments. The results presented here show that the alloy Ti-6Al-4V-0.5B satisfies all basic needs of a material for highly loaded permanent implants manufactured by MIM.

Introduction

Metal Injection Moulding (MIM) is a powder metallurgical technique aiming at the economic net-shape production of complex-shaped components in high quantity. The injection moulding process, well known from the processing of plastics, is exploited to form components with a very high degree of freedom with regard to geometry, without strongly influencing the production costs. Thus, bearing in mind medical implants, optimal functionality e.g. by anatomical shape can be provided. Because of the need of a rather expensive mould an economic benefit is gained typically at a total number of parts around some thousands. Thus, implants like bone screws, bone plates or dental implants could be good candidates for MIM manufacturing.

Improved functionality combined with lower costs can contribute to improving healing speed and well-being of patients and diminishing costs in public health. However, today MIM is still rather rarely applied for the production of medical devices and nearly no implants are manufactured by this technique.[1] On the one hand this situation is partly caused by insufficient knowledge of manufacturers and customers about the existence of this technology. But on the other hand, there are still drawbacks with regard to material properties. These are often connected to the fact that the microstructure of MIM processed materials differs from those of commonly used wrought materials. In order to understand this difference one has to regard that the processing chain of MIM is divided into shaping and compaction. Shaping is done by injection moulding as mentioned before. To meet the demands of the

moulding process a feedstock (fine metal powder blended with a polymeric binder) has to be produced and optimized. After shaping in a common plastic injection moulding machine the binder is removed from the green part and the metallic powder is compacted to a nearly dense material by a sintering process. This sintering gives rise to the difference in microstructure: 1. some residual porosity remains in the range of 1-3 % and 2. grain size and morphology change because sintering is a heat treatment.

Nevertheless, MIM of stainless steel is commercially performed since more than twenty years and the mechanical properties of the produced components are sufficient for most applications. However, a needed material for implants is titanium and its alloys and MIM of this material class is still rather new. The main challenge is the high affinity of titanium to oxygen and carbon. Even small amounts of these elements influence strength and ductility strongly.[2] Therefore, special requirements with regard to binder composition, processing of the fine powders and sintering have to be fulfilled, which exceed standard MIM processing. On the other hand, during the last years MIM processing of titanium and its alloys was highly improved [3-8] and commercial implants made from Ti-6Al-4V produced by this technology are available.[9]

Due to the residual porosity and a coarser microstructure the mechanical properties of MIM processed titanium tend to be somewhat poorer than those of standard wrought material, even though common ASTM standards can often be fulfilled. This is at least true in the case of static load. For cyclic load the situation appears to be worse, although only very little published data is available in this field.[10, 11] A recent study showed that processing Ti-6Al-4V by MIM leads to components with an endurance limit around 350 MPa in the as sintered stage without any surface treatment.[12] It has to be pointed out that this is still a reasonable

high value, but it is lower than the fatigue limit of wrought material which ranges typically between 500 and 800 MPa.[13]

In this paper a slightly modified Ti-6Al-4V alloy will be introduced as a possible new material for implants manufactured by Metal Injection Moulding. Under the given processing conditions of MIM the new alloy is optimised with regard to its fatigue behaviour. It is well known that a fine microstructure is beneficial for a good fatigue resistance. Therefore, boron, which is already used as a grain refiner for cast material in some studies, was added to the alloy powder. The microstructure of this new alloy and its mechanical properties are described. In addition, the new material is compared to standard Ti-6Al-4V, processed conventionally and by MIM, with respect to its corrosion behaviour and cellular reactions.

Experimental

Sample preparation

Samples were made from Ti-6Al-4V ELI material, also known as grade 23 according to ASTM B348, and from Ti-6Al-4V-0.5B, produced by blending of alloy powder with elemental boron powder as described below. From each of these materials four types of specimen were prepared, corresponding to the different investigations: 1. tensile test specimen according to ISO 2740 (“dog-bone-shape”) (**Figure 1a**); 2. cuboid-shaped samples for 4-point-bending fatigue tests (**Figure 1b**); 3. disc-shaped samples with a diameter of 30 mm and a height of about 2 mm for corrosion tests (**Figure 1c**) and 4. disc-shaped specimen with a diameter of 10 mm for biological tests (**Figure 1d**).

Nearly all specimens were made by MIM; however, for corrosion and biological tests reference samples were machined from standard wrought Ti-6Al-4V grade 23 material, provided by Enpar, Germany.

Feedstock production

Spherical, gas atomised Ti-6Al-4V ELI alloy powder from TLS Technik GmbH, Bitterfeld, Germany, with a maximum powder particle size of 45 µm and an oxygen content of 1100 µg/g was used. For the Ti-6Al-4V-0.5B material this alloy powder was mixed with elemental boron powder (grade I, 95 % purity) with a particle size < 2 µm, provided by H.C. Starck, Goslar, Germany, before feedstock production. As maximal impurity levels of the boron powder the following values were given by the supplier: 22,000 µg/g O, 4,000 µg/g N and 8,000 µg/g Mg. Binder components and powder were blended using a Z-blade kneader at a weight ratio of 1:9. All powder handling and feedstock production was performed under controlled argon atmosphere. As main binder components paraffin and a polyethylen derivative were used.

Injection moulding

Tensile test and 4-point-bending test samples were moulded on an Arburg 320S plastic injection moulding machine. Mass temperature was around 130 °C, maximum injection pressure amounted to 85 MPa. The corrosion specimens were moulded on a 100-KSA machine of MCP HEK, Germany, with a pressure of about 40 MPa. The samples for the biological tests were cut from the larger discs by means of a punch. This was done in the chemical debound state of the samples.

Debinding

The samples were chemically debound in heptane as solvent in order to extract the paraffin. Thermal debinding was carried out in the same furnace as sintering under Ar gas flow at around 450 °C.

Sintering

Sintering took place in a cold-wall furnace with molybdenum shieldings and tungsten heater. Pure Ti-6Al-4V samples were sintered at 1350 °C for 2h under high vacuum of less than 10^{-4} mbar, whereas for the specimens with boron addition 1400 °C was chosen in order to yield similar densification as discussed below.

Additional treatments

Some MIM-samples were exposed to an additional hot-isostatic-pressing process (HIP), performed by Bodycote HIP N.V., Belgium, at 915 °C for 2h at a pressure of 100 MPa in order to close the pores. This was done for investigating the influence of porosity on the mechanical properties.

All fatigue samples were shot peened under a pressure of 4 bar using zirconia particles with a diameter of 500 µm to ensure comparable surface quality. The tensile test specimens were tested as sintered. Corrosion samples were tested a) as sintered, b) as sintered and steam sterilised (20 min at 121°C and 2 bar) and c) as sintered and ground with SiC emery paper (1200er grid).

Mechanical tests and microstructure characterisation

Tensile tests were performed on a servohydraulic structural test machine equipped with a 100 kN load cell. The tensile tests were carried out at room temperature at a strain rate of 1.2 x 10^{-5} s^{-1}. At least three samples of each configuration were tested. The high-cycle four point bending fatigue tests were performed on a resonance machine fabricated by RUMUL

(Mikrotron 654-H, 20 kN). The experiments were carried out under load control with a cyclic frequency of ~95 Hz (sine wave) at a load ratio $R=\sigma_{min}/\sigma_{max}$ of 0.2. At least three samples were tested at each stress level. A fatigue endurance limit or "runout" for the tests was defined as 10^7 cycles. All experiments were conducted in air at room temperature. Light microscopy and scanning electron microscopy (ZEISS – DSM962) were used to investigate the microstructure. The level of interstitial elements (O, N, C) were determined using a LECO melt extraction system (TC-436AR and CS-444). The residual porosity was calculated from the density of the sintered samples, measured using the Archimedes method. Grain size was determined according to ASTM E112-96 [14] (linear intercept technique). Dilatometry measurements were performed under Ar atmosphere on MIM fabricated cylinders with a diameter of 5 mm, pre-sintered at 700 °C for 1h. A vertical configuration dilatometer fabricated by LINSEIS (L70/2171) was used. Electron backscatter diffraction (EBSD) was performed on a ZEISS (ULTRATM 55) scanning electron microscope equipped with a Hikari camera and TSL OIM Analysis 5.2 software. Spatially resolved EBSD maps were acquired at 15 keV using a step size of 0.2 µm. The samples were prepared by conventional polishing procedures followed by final polishing (5 min) with a Struers oxide polish suspension (OPS) compound. When electropolishing α+β titanium alloys, the β phase is attacked preferentially. This makes it impossible to detect the β phase and its texture during EBSD mapping. For this reason, the samples were finally polished in a vibratory machine (Buehler Vibromet 2) for 48 hours in a colloidal silica suspension (MasterMet® 0.06 µm).

Corrosion tests

The corrosion tests started with screening potentiodynamic polarisation measurements to study the influence of the surface condition of the specimens on the corrosion behaviour. In each case three specimens of the pure Ti-6Al-4V alloy and its boron alloyed variant (Ti-6Al-4V-0.5B) in the as sintered, sintered plus ground and sintered plus sterilised condition were

tested in Ringer solution at room temperature. The Ringer solution was composed of 8.6 g/L NaCl, 0.3 g/L KCl and 0.33 g/L $CaCl_2 \cdot 2H_2O$. More details of the polarisation measurements are given below in sequences 1 and 2.

In the framework of this study more detailed long-term tests at 37.2 °C could only be performed for as sintered and for ground specimens. Additionally a standard wrought Ti-6Al-4V alloy was tested to reveal any influence of the MIM process/microstructure on the corrosion behaviour. The latter was tested in two surface conditions (shot peened and ground). All electrochemical experiments were performed in Ringer solution, saturated with atmospheric oxygen. The corrosion cell (333 ml) with a three electrode set-up consisted of an Ag/AgCl reference, a Pt counter electrode and the specimen as working electrode. The electrolyte temperature was controlled at 37.2 ± 0.2 °C and the electrolyte was stirred during the experiments. One long-term experiment took a minimum of 3 days and consisted of three subsequent sequences as listed below.

1. 120 minutes recording of the free corrosion potential.

2. Potentiodynamic polarisation scan starting from -200 mV relative to the free corrosion potential with a scan rate of 0.2 mV/s. The test was terminated when a corrosion current of 0.1 mA was exceeded to minimize the damage on the specimen surface before the next sequence started. The corrosion rate was determined using the Tafel slopes.

3. Electrochemical impedance spectroscopy (EIS) measurements at free corrosion potential were carried out using a Gill AC over the frequency range from 10 kHz to 0.01 Hz. The amplitude of the sinusoidal signals was 10 mV. The measurements were repeated at

certain fixed times. The charge transfer resistance was estimated assuming a simple Randles circuit model.

For a second set of specimens the order of potentiodynamic polarisation and EIS measurements was reverted, thus starting with EIS directly after the free corrosion potential measurement.

Biological evaluation

Isolation and culture of cells

MG-63 cells

The human osteosarcoma cell line MG-63 was obtained from the European collection of cell cultures (ECACC, Salisbury, UK). The cells were cultured under standard cell culture conditions (37°C, 5% CO_2, 95% relative humidity) in Dulbecco's modified eagle medium (DMEM) Glutamax-I (Invitrogen Corporation, Karlsruhe, Germany) with 10% fetal bovine serum (FBS, PAA Laboratories, Linz, Austria). Cells were passaged at subconfluency (70 – 80%) and reseeded in a density of 2 x 10^4 cells/cm^2. For cell culture experiments cells after the 5^{th} passage were used.

RAW 264.7 Cells

The tumour-derived mouse macrophage cell line RAW 264.7 (ECACC, Salisbury, UK) was used as a model for cells derived from the immune system. Cells were cultured in DMEM low glucose with 2 mM glutamine and 10% FBS and passaged at 60-70% confluence. Cells starting from the 5^{th} passage were used for experiments.

Human umbilical cord perivascular cells (HUCPV)

Mesenchymal stem cells derived from Wharton`s jelly of the umbilical cord were isolated by a modified isolation protocol.[15] Isolation was approved by the local ethical committee. In brief, umbilical cords from consenting full-term caesarean section patients were cut into pieces of about 5 cm. The vessels from the cord pieces were isolated and tied together at the ends with sutures, leading to a vessel loop. These were placed in T-175 cell culture flasks and cultured for 10 days without medium change in α-MEM (Invitrogen Corporation, Karlsruhe, Germany) with 10% FBS for mesenchymal stem cells (Stem Cell Technologies, Vancouver, Canada). After visible outgrowth from the loops medium was changed every 2-3 days. At about 60% confluency the cells were harvested with a cell scraper and subcultivated in a density of 1000 cells/cm^2. For the experiments cells of the third to fifth passage were used.

Human bone derived cells (HBDC)

HBDC were grown out of bone chips obtained from patients undergoing total hip arthroplasty following the protocol of Gallagher.[16] Isolation was approved by the local ethic committee. In brief, cancellous bone was cut into pieces of about 5 mm. After removal of bone marrow and adjacent cells by vigorous vortexing the pieces were cultured in Dulbecco´s modified eagle medium (DMEM) Glutamax-I (Invitrogen Corporation, Karlsruhe, Germany) with 10% fetal bovine serum (FBS, PAA Laboratories GmbH, Linz, Austria), 1% penicillin and 100 µg/ml streptomycin (Invitrogen Corporation, Karlsruhe, Germany) for about ten days without medium change. At visibility of outgrowing HBDC, medium was changed every three days. Passaging was done at 70 – 80% confluence. Experiments were performed with cells in the 1st passage.

Cytotoxicity assay of boric acid

To evaluate a possible cytotoxic effect of boric acid, a cytotoxicity assay was performed.[17] RAW 264.7, MG-63 or HUCPV cells were seeded in 96-well plates (Nunc, Wiesbaden,

Germany) in a density of 2 x 10^3 per well/100 µL and incubated at 37°C for 24 hours to allow cell adhesion. Thereafter, boric acid (99.999%, Sigma-Aldrich Chemie, Taufkirchen, Germany) in different concentrations (range 1-200 mM) was added. After another 48 hours incubation time, cell viability was measured by MTT (methylthiazolyldiphenyl-tetrazolium bromide). In brief, 10 µL of the MTT-solution (5 mg/mL MTT in phosphate buffered saline PBS) was added and after an incubation period of 5 hours the cells were lysed and the formazan crystals solubilised by adding 1 mL solubilization solution (10% SDS in 0.01M HCl; Merck, Darmstadt, Germany), followed by an incubation overnight in a humidified atmosphere (37° C, 5% CO_2). The solubilised formazan product was photometrically quantified using an ELISA reader (Tecan Sunrise, TECAN Deutschland GmbH, Crailsheim, Germany) at 570 nm with a reference wavelength of 655 nm. The same experiments were performed without cells to exclude an influence of the salt concentrations on the MTT-assay. For each concentration 16 replicates were performed. Tissue culture plastic (TCP) was used as positive control. Experiments were repeated at least three times.

To determine significant influences of the added elements on the different cell types two markers were used. On one hand the half-lethal dose (LD_{50}) was used as a measure for the concentration capable of killing half of the seeded cells. On the other hand the initial inhibitory concentration (IIC) was calculated, which is derived from the statistical analysis (ANOVA vs. control group, Dunn's or Dunnet's post hoc test, see section Statistics). This value indicates the first significant negative deviation from the viability data obtained from the untreated control group.

Cell adhesion after 1 and 3 hours

To compare the initial adhesion of primary cells, HBDC and HUCPV were used. 100000 cells in 50 µL medium were seeded on the different materials in 12-well plates and left for

adhesion for 30 min. Thereafter the samples were incubated in 3 mL medium for the remaining time. After the incubation time the samples were transferred into new wells containing trypsin / EDTA solution and incubated for 5-10 min on a shaker to remove the adhered cells. Cells were counted using a CASY TT cell counter (Roche Innovatis GmbH, Reutlingen, Germany). Each material was tested in 8 replicates. Values were calculated as percent of initially seeded cells.

Additionally, HBDC adhesion on Ti-6Al-4V-0.5B after 1 and 3 hours was visualised by scanning electron microscopy. 3×10^4 cells in 50 µL medium were applied to the carriers in agarose-coated wells to minimize adhesion to tissue culture plastic (TCP). After 30 min to allow initial adhesion, the carriers were covered with 2 mL DMEM. The specimens were incubated for one or three hours before sample preparation for microscopy. Briefly, after dehydration (isopropanol gradient), samples were critical point dried with an EM CPD030 (Leica, Wetzlar, Germany). Samples were then examined using a scanning electron microscope Auriga (Zeiss, Oberkochen, Germany), operating with a secondary electron detector (SE) in low voltage field emission mode at 0.7 and 1.5 kV.

Proliferation of HUCPV

Cell proliferation was analysed by seeding 50000 cells on the carriers as described before. Proliferation times were 5, 10 and 15 days, respectively. Thereafter cell viability was measured by MTT. Experiments were performed with 6 samples per material and repeated three times.

MG-63 viability

The viability measurements were done in a 6-fold redundant assay for Ti-6Al-4V and for Ti-6Al-4V-0.5B samples, and in a 3-fold redundant assay for the positive control (TCP). MG-63

cells were applied in a density of 5×10^4 cells in 50 µL medium directly on TCP and on the carriers in agarose-coated wells. After 30 min to allow initial adhesion, the carriers were covered with 2 mL DMEM. The specimen were incubated for three days before MTT (cell proliferation kit MTT; Roche Diagnostics GmbH, Mannheim, Germany) assays were performed. The MTT procedure was followed as outlined in the manufacturer's protocol. Briefly, 100 µL of the MTT-solution (5 mg/mL MTT in PBS) was added to cell supernatant. After an incubation period of 5 h the cells were lysed and the formazan crystals solubilised by adding 1 mL solubilisation solution and incubation overnight. The solubilised formazan product was photometrically quantified using an ELISA reader (Tecan Sunrise, TECAN Deutschland GmbH, Crailsheim, Germany) at 570 nm with a reference wavelength of 655 nm. Concomitant LIVE/DEAD® cell viability stainings (Invitrogen, Karlsruhe, Germany) were performed for cells on both carriers after three days. This technique relies on a dual staining of viable (green; membrane-permanent calcein-AM) and membrane-compromised (red; membrane-impermeant ethidium homodimer) cells. Results were documented with a fluorescence microscope (Eclipse Ti-S, Nikon, Düsseldorf, Germany).

Statistical analysis

Statistics were performed using the SigmaStat package (Systat software GmbH, Erkrath, Germany). For the analysis of dose effects stepwise regression analysis was performed. Standard analysis comparing more than two treatments was done by using the one-way ANOVA. Depending on the data distribution either a one-way ANOVA or an ANOVA on ranks was performed. Post-hoc tests were Holm-Sidak or Dunn's versus the control group, respectively. Statistical values are indicated at the relevant experiments.

Results and Discussion

In the following, samples fabricated by MIM from Ti-6Al-4V and Ti-6Al-4V + 0.5B powders are referred to as *MIM Ti64* and *MIM Ti64-B*, respectively. Wrought alloy will be denoted as *wrought Ti64*.

Microstructure

The microstructure of the wrought Ti64 alloy used as reference material for corrosion and biological tests is shown in **Figure 2a**. It consists of equiaxed alpha-grains of hexagonal-closest-package structure with body-centred-cubic beta-phase at the grain boundaries, which is shown in the inset in higher resolution. The average diameter of the alpha grains was determined as 5 µm. In comparison **Figure 2b** displays the much coarser microstructure of the same material, but processed by MIM. Sintering took place at 1350 °C for 2h above the beta-transus temperature of around 1000 °C. In this pure beta-region the grains grow rather easily and during furnace cooling alpha-phase is formed at falling below the beta-transus temperature again. The result is a lamellar microstructure with a colony size around 148 µm. Compared to the grain size of the wrought material this value is much higher. Thus, it can be assumed that at least strength and endurance limit of the MIM processed material will be significantly lower. The samples exposed to an additional HIP process reveal the microstructure shown in **Figure 2c**. As to **Table 1** after HIP the grain size remains nearly constant, but the pores are closed completely.

In contrast to MIM-Ti64 the microstructure of the MIM-Ti64-B material is significantly different (**Figure 2d**). There is nearly no lamellar structure visible anymore and the overall structure appears to be finer compared to Figures 2b and 2c. In fact, the grain size is reduced to below 20 µm (**Table 1**).

The different microstructure of the boron added alloy is caused by the formation of titanium borides visible in Figure 2d as middle gray needle–like features. The evaluation of Kikuchi patterns during EBSD measurements analysed the composition to be TiB. No TiB_2 could be detected. Feng et al.[18] stated that TiB is in situ synthesized by means of solid state diffusion between Ti powder and boron powder. Moreover, the TiB particles are formed by the one-way diffusion of B atoms primarily along the $[010]_{TiB}$ direction. Consequently, the needle-shape morphology of the TiB particles is associated to the faster diffusion rate in one direction.[19] Other investigations[20] showed that the particles are formed at around 800 °C by reaction of the elemental boron with the titanium in the alloy powder. Because boron is a very fast diffuser in alpha titanium the powder particles interact quickly during heating up. Dilatometry measurements confirm this assumption (**Figure 3**). The linear shrinkage rate shows a significant drop at around 820 °C which can be related to the formation of borides.

Titanium borides are known as effective grain refiner in the frame of casting added as fine particles to the melt.[21] In that case they both influence the nucleation process during solidification and act as obstacles for grain growth via grain boundary pinning. In addition, during cooling alpha-phase nucleates at the particles leading to more and smaller alpha grains. In the case of MIM the two latter mechanisms appear to work, too. During sintering in the beta region the growth of the beta grains is impeded by pinning the grain boundaries by the titanium boride particles. EBDS images of the beta phase which are not shown here confirm this assumption; the comparison of MIM-Ti64 and MIM-Ti64-B reveals the much larger region of same orientation in the case of the MIM-Ti64 material, which is assumed to be the size of the original beta grains. After cooling many small alpha grains are visible in the case of MIM-Ti64-B as displayed in **Figure 4**. This is contrary to the lamellar structure of the pure Ti64 alloy processed by MIM. It can be assumed that the TiB particles act as centres for

heterogeneous nucleation during cooling below the beta transus temperature as described before.

Table 1 shows the measured data of the MIM samples concerning porosity, grain size and content of O, N and C. A density of 4.41 $g \cdot cm^{-3}$ for the dense material was determined by measuring a MIM+HIP sample. It is important to point out, that the addition of boron improves the final densification although the shrinkage is delayed compared to MIM Ti64 as visible in Figure 3. On the other hand, after this delay the maximum shrinkage rate exceeds that of MIM Ti64 significantly, if the temperature is high enough. Therefore, a sintering temperature of 1400 °C was chosen to accelerate diffusion which appears to be impeded by the boride particles. On the other hand, in the end the pinning of the grain boundaries leads to a better densification due to the fact that the pores remain at the grain boundaries where fast diffusion is guaranteed. This is different compared to the situation when grain coarsening occurs during sintering, effecting a virtual shift of the pores into the grains where diffusion is much slower.

Mechanical properties

Table 2 displays the result of the tensile tests performed on the MIM samples. For comparison also the requirements corresponding to ASTM standard B348 grade 23 are given. The table reveals that the strength of pure MIM-Ti64 is slightly too low to fulfil the requirements of the standard, while the ductility exceeds the minimum value significantly. On the other hand, the MIM-Ti64+HIP specimen fulfil all standard requirements clearly. Taking into account the microstructural features (Table 1) it can be concluded that the reason for this behaviour is the elimination of the porosity by the HIP process. The interstitial contents of MIM-Ti64 and MIM-Ti64+HIP are nearly identical and the difference in grain size would contribute into the opposite direction, if there would be any effect. Also the mechanical

properties of the boron added alloy fulfil the standard requirements. The increase in strength is probably due to the significantly finer microstructure, while the slight loss of ductility is caused by the TiB particles. As shown in Table 1 the oxygen content of MIM-Ti64-B is slightly lower than that of MIM-Ti64, though, the strength is higher.

The results of the fatigue tests are given in Table 2, too, and are shown in **Figure 5**, where the Wöhler curves of the tested samples are drawn. The figure shows that closing of the porosity increases the endurance limit by about 50 MPa (Table 2). On the other hand, the refinement of the microstructure effects an improvement by 190 MPa, despite of a residual porosity of 2%. The connection between grain size and fatigue behaviour is well known and confirmed by this study. Thus, the endurance limit of MIM-Ti64-B is situated well in the middle of the typical range of wrought material, while that of MIM-Ti64+HIP is just next to the lower end.

Corrosion behaviour

Measurements at room temperature

Typical results of the potentiodynamic polarisation measurements on the MIM processed samples are displayed in **Figure 6** and the evaluation of all measurements is given in **Table 3**. It is obvious that the electrochemical properties are dominated by the oxide film on the surface and under which conditions the film was formed during processing or pre-treatments. Thus, there is a major influence of the surface condition on the corrosion behaviour.

In the as MIM condition, the oxide film is rather thick but non-uniform. This has the consequence that the free corrosion potential is shifted to the noble direction and the current increase is retarded during anodic polarisation. However, due to larger imperfections the breakthrough potential is rather low and varies strongly from measurement to measurement. If

the original as MIM surface is removed e.g. by grinding and if there is enough time between the removal and the corrosion test (more than 2 days) a fresh and obviously more uniform oxide film can form again. This layer is thinner and thus, less noble free corrosion potentials are recorded and current increase can be noticed earlier at lower polarisation potentials.

However, the film growth during anodic polarisation appears to be denser and thus the lowest current densities in the passive range can be recorded comparing the three different surface conditions. However, the thinner oxide layer thickness is most likely responsible for a lower break through potential compared to the sterilized surface condition.

The sterilization process may remove impurities and imperfection in the as MIM surface state, while the overall thickness is not much affected. The result is the highest break through potential (> 3000 mV) of all three different surface conditions. Please note that for the sterilized surfaces no break through potential could be recorded due to the limitations of the used potentiostat. Interestingly the sterilized surface reveals a strong increase in the current density in the region from about 1300 to 1600 mV. This might be attributed to the decomposition of water or the reduction of chloride ions. However, the following decrease in current density with further increasing polarisation potential may indicate that the water decomposition is the main process with the resulting oxygen stabilizing the passive film again. This current peak in the potential – current curve is in a much weaker form also visible in the grinded but not in the as MIM condition suggesting that the as MIM surface is either somehow suppressing the decomposition or more likely the decomposition process is starting softly without the sharp increase.

Looking at the influence of the alloy composition one can state that the influence of the boron addition on the corrosion behaviour is only marginal. The boron seems to have a minor

influence on the oxidation behaviour which seems to be slightly enhanced in the presence of boron. If anodically polarized the passive current density of MIM Ti64-B is always slightly higher than for MIM Ti64 independent of the surface condition. In the as MIM condition the easier oxide formation may result in a denser layer formation during processing which may have a beneficial influence on the corrosion resistance. Impurities are better embedded in a thicker oxide layer and imperfections are more easily levelled. Thus, lower corrosion rates are found for the boron alloyed specimens. In the other two surface conditions pretreatments have cleaned the surface and it is more beneficial if a thin more protective oxide layer is growing rather than a thicker one that may be able to embed impurities. In that sense the corrosion rates determined for MIM Ti64 are slightly lower compared to the boron containing counterparts. However, it should be stated that the difference is only small and the overall corrosion performance in Ringer solution is good regardless the presence of boron or not in the alloy.

Measurements at 37.2 °C

Free corrosion potential

The as sintered surfaces of the MIM specimen reveal no clear trend in the corrosion potential (**Figure 7**). There are large variations within the same set of specimens which might be a result of deposits on the surface during sintering. The largest variations are observed for MIM Ti64 followed by MIM Ti64-B specimens. The wrought specimens with a shot peening finish reveal no major variations in the potential indicating that peening is able to produce a uniform and reproducible surface state. Nevertheless the values are still different from a more or less pure and clean condition which can be expected if the surface and any contaminations are removed by sufficient grinding. After grinding all potentials are within the same region: -278 mV for MIM Ti64, -282 mV for MIM Ti64-B and -273 mV for wrought Ti64. Those values were obtained from specimens which were immersed in the Ringer solution

immediately after the grinding of the surface, thus the oxide layer is obviously still thin and does not affect the potential too much. In contrast to the screening tests at room temperature the potential in the beginning is not shifted to the passive region and closer to values which one would expect for a free titanium metal surface.

Polarisation

The results indicate that all specimens except the shot peened remain passive in the solution. Similar to the room temperature results, the specimens are obviously all protected by the native oxide layer on the titanium surface. Only the shot peened specimen is most likely contaminated by noble metal impurities introduced by contaminations in the shot, thus dissolving directly after passing the corrosion potential (**Table 4**). Thus it is no surprise that the corrosion rate determined by Tafel slope evaluation is the highest of all as received specimens. However, also the best corrosion performance was obtained for the wrought Ti64 material, simply by cleaning the surface by grinding, supporting the idea of surface contaminations. Comparing the MIM specimens MIM Ti64 has a slightly lower corrosion rate than MIM Ti64-B which is consistent with the room temperature findings. In contrast to the wrought Ti64 grinding (cleaning) of the surface of MIM specimen results in a reduced corrosion resistance indicating that the sintered surface is more resistant than a clean pure surface. This is also obvious in the potential-current plots revealing that the protective film on all ground specimens start to fail at about 2400 mV while the MIM specimen remain passive until 3000 mV. Furthermore the differences in the passive current between the two MIM alloys are much smaller in the as sintered condition compared to the ground condition suggesting a similar surface after sintering. However, in the bulk of the specimens the boron addition results in a reduced corrosion resistance, although the overall performance is still good. In spite of the lower break through potential the performance of the clean wrought Ti64 material is the best. Interesting to note is an increase in the current density for all specimen if

a potential of about 1200 mV is passed. This again might be related to decomposition of water and/or the reduction of chloride ions. The temperature influence on the corrosion resistance is only minor. There is an improvement for the as MIM condition by a factor of two reduced corrosion rate and a reduced passive current as well. The ground conditions behave more as expected with similar corrosion rates but increasing passive current densities with increasing temperature.

EIS

The long-term EIS measurements reveal that there is almost no change in the impedance response of the MIM specimens due to the immersion in Ringer solution (**Figure 8**). This suggests that the surface films are neither increasing their thickness/stability nor are they dissolving or locally failing. Only the resistance of MIM Ti64-B is lower than MIM Ti64 confirming the polarisation results. Even the EIS measurements performed after the polarisation scans do not reveal remarkable different impedance values although one may expect a thicker oxide layer because of the previous anodic polarisation (not shown).

Biological properties

Cellular reaction to boric acid

Cytotoxicity measurements of elemental boron (supplied as boric acid) were performed due to a possible release of boron from the material after implantation. Three different cell types were chosen as model systems for bone (MG-63), primary mesenchymal cells (HUCPV) and cells from the immune system (RAW 264.7). These are the cell types which will get in contact with the implant material subsequently after implantatation.All cell types showed a typical dose-response curve (**Figures 9 a-c**). RAW cells showed the lowest tolerance for boric acid. The initial inhibitory concentration (IIC) was 2 mM and the LD50 was at 7 mM. MG-63

tolerated slightly higher boron concentrations (IIC=3 mM; LD50=29 mM), whereas HUCPV did not reach the half-lethal dose in the measured concentration range, although the IIC was 6 mM. This ranking of cell tolerance was also observed in other studies, and it is due to the nature of the used cells. Many cell lines are derived from cancers, and the cells seem to be more sensitive to certain substances (e.g. rare earth elements). [17, 22] In contrast, primary cells are more difficult to obtain, but they show lower sensitivity to this substances in vitro. The applied concentration range of boric acid was quite high. Even if all boron would be released from the material these concentrations would not be reached. Boron additionally is an essential element in plants and it is assumed to be essential also for humans.[23] The acute lethal dose of boron by accidental poisonings is 3000-6000 mg for infants and 15000 – 20000 mg for adults.[24] Taking the experimentally determined corrosion rate and the formation of TiB-phases into account the amount of possibly released boron is neglectable.

Cell adhesion

The initial cell adhesion after one and three hours was different for both primary cell types. HUCPV showed no significant differences in cell adhesion between the different materials. However, slightly more HUCPV adhered to the wrought material after 1 hour, whereas after 3 hours the boron containing sample was favoured (**Figure 10 a**). In contrast, human bone derived cells, which are the most relevant cell type for bone showed a significantly higher adherence on both MIM materials compared to the wrought Ti64 at 1 and 3 hours, with the highest preference for MIM Ti64-B (one way ANOVA, Holm-Sidak post hoc test, $p<0.05$; **Figure 10 b**). Cell adhesion behaviour also differed very much between both cell types. A fraction of at least 60% of the seeded HUCPV was adherent already after 1 hour, and this value tended to decrease for wrought Ti64 and MIM Ti64. This indicates that HUCPV are adhering fast, but not all of the initially adherent cells are staying on the material. In contrast, bone derived cells adhered more slowly and the number of adherent cells increased over time.

Therefore they may be a better indicator for surface quality during early adhesion. Additionally, SEM examination of HBDC adhesion after one and three hours highlights the affinity of the human bone derived cells for the MIM Ti64B. Already after one hour, some membrane protrusions are visualised (**Figure 11, A and B**), but the cells remain rounded. However, after 3 hours HBDC exhibit a flattened, elongated morphology, characteristic of osteoblast cells (**Figure 11, C and D**). There were no differences in the cell shape after full adhesion between the samples.

HUCPV proliferation

Cell proliferation of HUCPV was measured by MTT after 5, 10 and 15 days (**Figure 12**). On the fifth day a significantly lower adhesion was determined on MIM Ti64 compared to the other materials (one-way ANOVA, Holm-Sidak Post-Hoc test, $p>0.05$). At the later days no significant differences were observed. However, the highest MTT-values were found on MIM Ti64-B in all measurements. After 15 days all materials showed a similar performance for cell proliferation.

MG-63 viability

No statistical difference was observed for osteoblast- like cell MG-63 viability on MIM Ti64 or MIM Ti64-B compared to the control (**Figure 13**). A slight viability decrease can be discerned for MIM Ti64-B. However, less dead cells were distinguished with the dual staining for MIM Ti64-B compare to MIM Ti64. This difference can be explained by the inherence of the tests themselves. MTT assay, the most common assay for tetrazolium salt–based viability test, depends on cell metabolism and on cell proliferation, abrogating the living, but non-metabolically active cells. Therefore, based on the dual-staining assay, more living cells were observed on MIM Ti64-B substrate, confirming its higher cell compatibility.

Based on the cell adhesion and proliferation results the boron containing titanium alloy exhibits the most favourable cellular reaction. This is most likely due to the different microstructure of the samples, which will also result in varying surfaces. The microstructure of the surface is highly important for all cell functions including adhesion, proliferation and differentiation.[25-27] As depicted in **Figures 14 to 16** the surface of the MIM samples is not comparable to e.g. polished wrought titanium alloy surfaces. Besides the presence of grooves on the surface it can also be observed, that by the sintering process a microstructure is introduced, which additionally favours early osteoblast adhesion. The sintered surface is characterised by smooth roughness in connection with an increase of the surface area. In further studies the influence of this surface structure on proliferation and differentiation of bone-derived cells will be analyzed in more detail.

Conclusions

The results of this study show that the titanium alloy Ti-6Al-4V-0.5B processed by Metal Injection Moulding is well suited as a material for medical implants under high load. The mechanical properties fulfil the ASTM standard for Ti-6Al-4V ELI wrought material. Furthermore, the fine microstructure, which is caused by the addition of boron, leads to a fatigue limit of 640 MPa under 4-point-bending test condition. This value is equivalent to that of wrought material.

Alloying the Ti-6Al-4V alloy with boron results in a slightly reduced corrosion resistance. The reason however is not clear as the microstructure is changing remarkable by the boron addition (grain size is reduced, phase fractions are changing and a new TiB-phase appears). Titanium boride is a new phase that forms and which may cause galvanic corrosion effects (although the effect is not high) and grain size together with phase fraction changes may have

effects on the corrosion resistance as well. A change in the corrosion mechanisms due to the B addition was not noticed. Both specimens showed still a low and uniform general corrosion of the surface.

The as sintered surface of MIM specimens is more corrosion resistant than the bulk of MIM specimens.

All Ti-6Al-4V and Ti-6Al-4V-0.5B materials investigated are stable in Ringer solution as long as they are free from contaminations.

The corrosion resistance of MIM processed Ti-6Al-4V appears to be reduced compared to the same conventional wrought alloy. However this might be only an artefact due to the inherent porosity in the MIM specimens which can not be considered by the calculation of the surface area exposed to the electrolyte.

Cell adhesion and proliferation data indicate an increased initial adhesion and slightly improved proliferation profile for the boron containing material. In combination with the mechanical and corrosion properties the MIM processed Ti-6Al-4V-0.5B alloy therefore could be a suitable material for biomedical applications based on the MIM process.

Acknowledgements

The authors wish to thank Daniel Laipple for the perfect help with operating the SEM.

Received: ((will be filled in by the editorial staff))
Revised: ((will be filled in by the editorial staff))
Published online: ((will be filled in by the editorial staff))

References

_[1] T. Ebel, Powder Injection Moulding International, Vol.2 (2008) 2, 21

_[2] H. Conrad, Acta Metallurgica 14 (1966) 1631

_[3] Y. Itoh, T. Harikou, K. Sato, H. Miura, Proceedings PM World Conf. 2004, Vol. 4, EPMA, Shrewsbury (2004), 445

_4] R. Zhang, J. Kruszewski, J. Lo, Powder Injection Moulding International, Vol.2 (2008) 2, 74

_[5] E. Nyberg, M. Miller, K. Simmons, K. S. Weil, Mat. Sc. Eng. C 25 (2005) 336

_[6] S. Guo, X. U, J. Xiang, R. Ang, X. He, M. Li, S. Duo, W. Li, Trans. Nonferrous Met. SOC. China 16 (2006) 701

_[7] G.C. Obasi, O.M. Ferri, T. Ebel, R. Bormann, Mat. Sci. Eng. A 527 (2010) 3929

_[8] E. Aust, W. Limberg, R. Gerling, B. Oger, T. Ebel, Advanced Engineering Materials. Vol. 8 (2006) 5, 365

_[9] B. Oger, T. Ebel, W. Limberg, Proceedings EUROPM 2006, Vol 2., EPMA, Shrewsbury (2006), 191

_[10] M. Niinomi, T. Akahori, M.Nakai, K. Ohnaka, Innovations in titanium technology, Proceedings TMS2007 (2007), 209

_[11] P.V. Muterlle, A.Molinari, M. Perina, P. Marconi (2010), PM2010 Proceedings Volume 4, Shrewsbury, EPMA, 791

_[12] O.M. Ferri, T. Ebel, R. Bormann, Mat. Sci. Eng. A 504 (2009) 107

_[13] C. Leyens, M. Peters, Titanium and titanium alloys, Wiley-VCH, 2003

_[14] ASTM standard E112-96, “Standard Test Methods for Determining Average Grain Size”, ASTM International, West Conshohocken, PA, 2004

_[15] R. Sarugaser, D. Lickorish, D. Baksh, M. M. Hosseini, J. E. Davies, Stem Cells 2005, 23, (2), 220

_[16] J.A. Gallagher, Methods Mol Med 2003, 80, 3

_[17] F. Feyerabend, J. Fischer, J. Holtz, F. Witte, R. Willumeit, H. Drücker, C. Vogt, N. Hort, Acta Biomaterialia 2010, 6, (5), 1834

_[18] H. Feng, Y. Zhou, D. Jia,, Q. Meng, Material Science and engineering A 390, 2005, 344-349.

_[19] K.B. Panda and K.S. Ravi Chandran, Metallurgical and Materials Transactions A 2003, 34, (6), 1371-1385

_[20] S.V. Divinski, F. Hisker, T. Wilger, M. Friesel, C. Herzig, Intermetallics 16 (2008) 148

_[21] M.J. Bermingham, S.D. McDonald, K. Nogita, D.H.ST. John, M. S. Dargusch, Scripta Materialia 59 (2008) 538

_[22] Feyerabend, F.; Siemers, C.; Willumeit, R.; Rosler, J., Cytocompatibility of a free machining titanium alloy containing lanthanum. J Biomed Mater Res A 2009, 90, (3), 931-9.

_[23] Jensen, A. A., Risk assessment of boron in glass wool insulation. Environ Sci Pollut Res Int 2009, 16, (1), 73-8

_[24] Expert Group on Vitamins and Minerals, Safe Upper Levels for Vitamins and Minerals; 2003

_[25] D. Perizzolo, W.R. Lacefield, and D.M. Brunette, J Biomed Mater Res 2001, 56, 494

_[26] N.R. Washburn, K.M. Yamada, C.G. Simon, Jr., S.B. Kennedy, and E.J. Amis, Biomaterials 2004, 25, 1215

_[27] K. Anselme, M. Bigerelle, B. Noel, E. Dufresne, D. Judas, A. Iost, and P. Hardouin, J Biomed Mater Res 2000, 49, 155

Table 1. Microstructural data of the MIM processed samples.

Material	Porosity [%]	grain size [µm]	O [µg/g]	N [µg/g]	C [µg/g]
MIM-Ti64	3.6	148 ± 20	2318 ± 44	172 ± 24	409 ± 23
MIM-Ti64+HIP	0.0	174 ± 26	2308 ± 16	177 ± 5	480 ± 7
MIM-Ti64-B	2.3	18 ± 5	1960 ± 21	164 ± 6	390 ± 66

Table 2. Mechanical data of the MIM processed samples.

Material	YS [MPa]	UTS [MPa]	ε_f [%]	Endurance limit
MIM-Ti64	720 ± 2	824 ± 4	13.4 ± 0.7	450
MIM-Ti64+HIP	841 ± 5	937 ± 3	17.1 ± 2	500
MIM-Ti64-B	787 ± 1	902 ± 3	11.8 ± 1	640
ASTM B348 Gr. 23	> 760	> 825	> 10.0	n.a.

Table 3. Electrochemical properties of the two MIM processed alloys (Ti-6Al-4V and Ti-6Al-4V-0.5B) in the three surface conditions determined from potentiodynamic polarisation measurements in Ringer solution at room temperature.

Material, surface condition	Corrosion rate [µm·y^{-1}]	Free corrosion potential [mV]	Passive Current 1 [µA·cm^{-2}]	Passive Current 2 [µA·cm^{-2}]	Break through potential [mV]
MIM Ti64	0.67 ±0.06	131.3 ±12.4	1.47 ±0.03	-	1856 ±611
MIM Ti64-B	0.39 ±0.08	140.1 ±7.6	1.58 ±0.07	-	2727 ±222
MIM Ti64 ground	0.32 ±0.12	65.3 ±15.1	1.1 ±0.06	1.76 ±0.12	2543 ±26
MIM Ti64-B ground	0.39 ±0.11	85.8 ±16.6	1.18 ±0.005	1.78 ±0.1	2777 ±47
MIM Ti64 sterilized	0.41 ±0.12	156.4 ±4.3	1.42 ±0.03	1.83 ±0.08	> 3000
MIM Ti64-B sterilized	0.53 ±0	185.4 ±15.9	2.1 ±0.1	3.77 ±2.36	> 3000

Table 4. Electrochemical properties of the two MIM processed alloys (Ti-6Al-4V and Ti-6Al-4V-0.5B) in comparison with wrought Ti-6Al-4V alloy determined from potentiodynamic polarisation measurements in Ringer solution at 37.2°C.

Material, surface condition	Corrosion rate [$\mu m \cdot y^{-1}$]	Free corrosion potential [mV]	Passive Current 1 [$\mu A \cdot cm^{-2}$]	Passive Current 2 [$\mu A \cdot cm^{-2}$]	Break through potential [mV]
wrought Ti64 shot peened	0.75 ±0.12	-125 ±3	-	-	-
wrought Ti64 ground	0.09	-273	0.69	1.16	2413
MIM Ti64	0.15 ±0.03	-58 ±76	0.95 ±0.04	1.61 ±0.17	>3000
MIM Ti64-B	0.22 ±0.01	19 ±19	1.08 ±0.03	2.15 ±0.15	>3000
MIM Ti64 ground	0.29	-278	1.03	2.38	2346
MIM Ti64-B ground	0.32	-282	2.38	3.52	2367

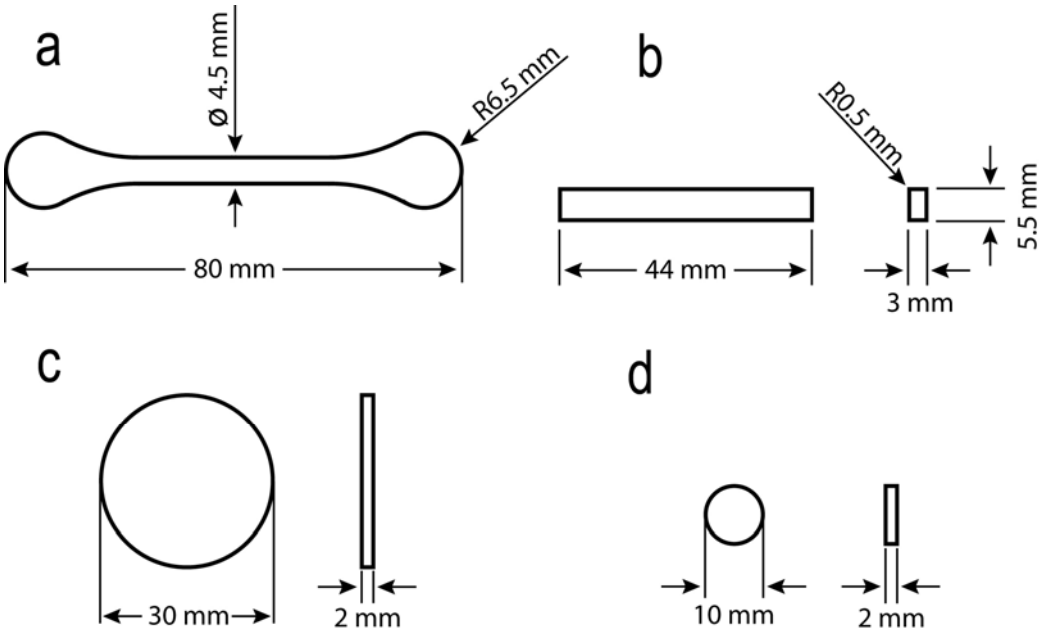

Fig. 1. Specimen geometries of the sintered parts, for a) tensile tests, b) fatigue tests, c) corrosion tests and d) biological tests. Dimensions are given as typical values. The exact dimensions depend on the sintering conditions affecting the shrinkage.

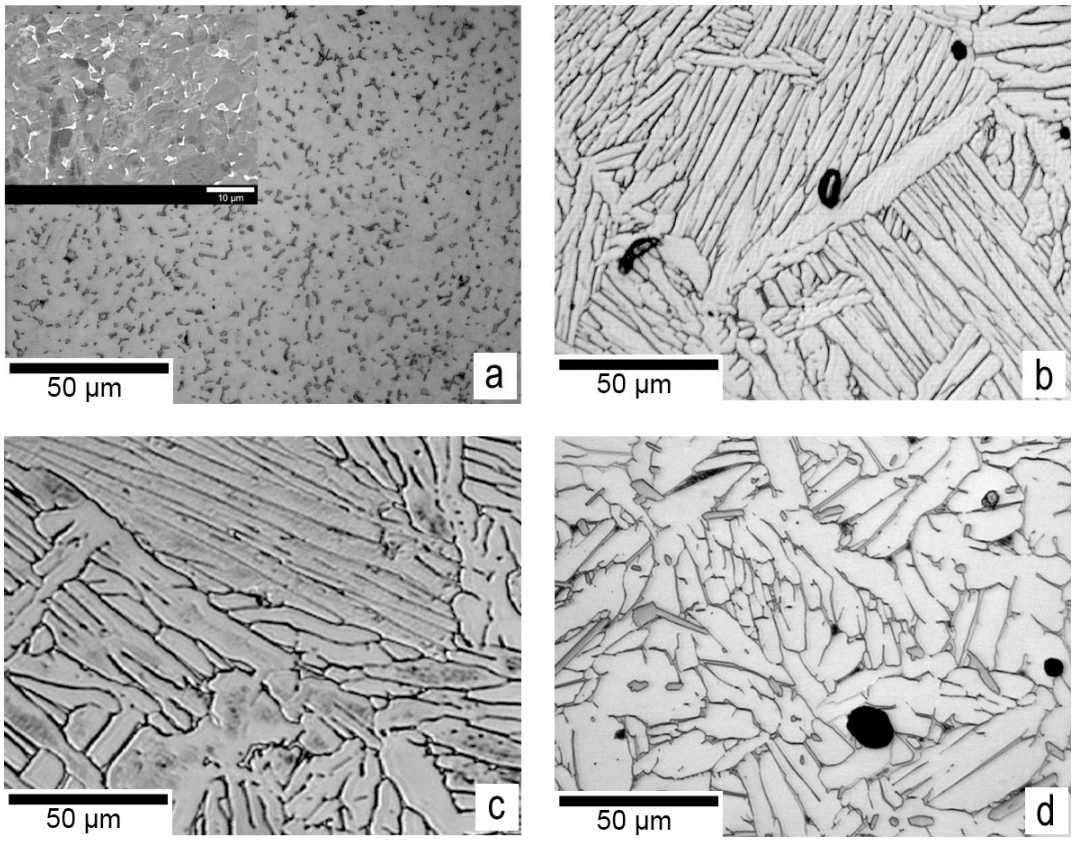

Fig. 2. Microstructure images of Ti-6Al-V4 material (a-c), differently processed, and Ti-6Al-4V-0.5B (d). a) wrought material (image plane perpendicular to rolling direction), b) MIM material, c) MIM and additional treated by hot-isostatic pressing (HIP). Images made by light microscopy.

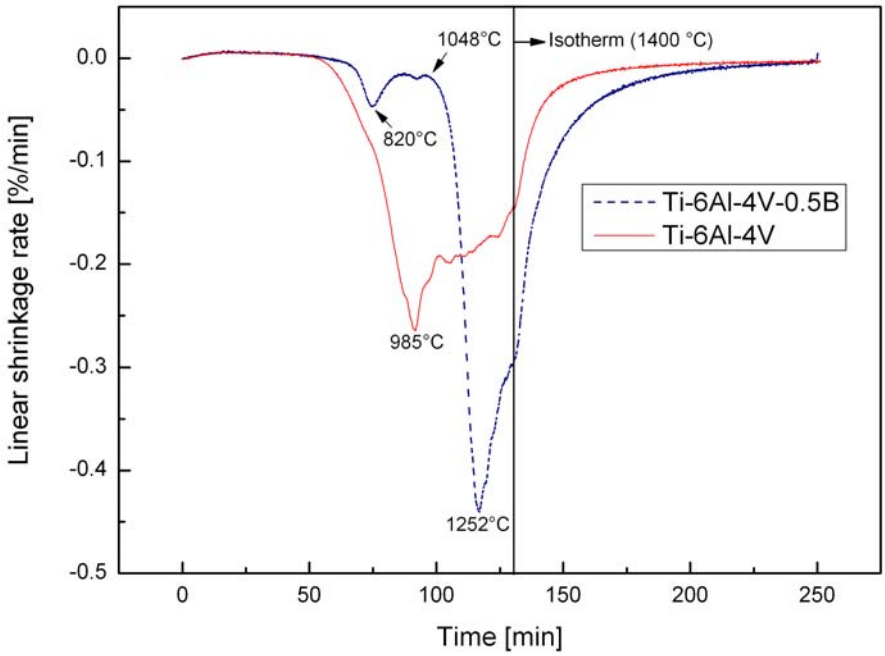

Fig. 3. Shrinkage rate of MIM64 and MIM64-B measured by dilatometry. The drop at 820 °C is assumed to be related to the formation of titanium borides. It is worth to notice, that the maximum shrinkage rate is significantly higher in the case of the boron added alloy.

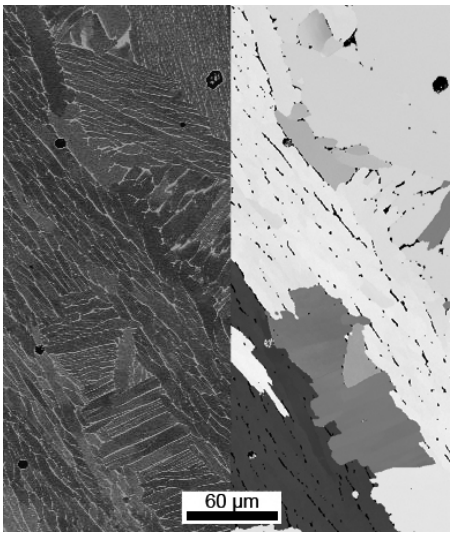

Fig. 4a. MIM Ti64

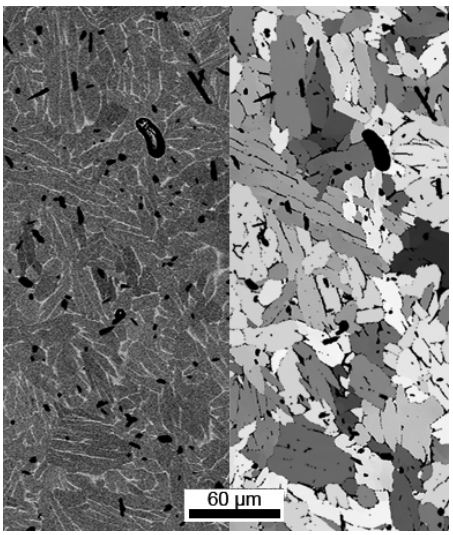

Fig. 4b. MIM Ti64-B

Fig. 4. BSE (left) and EBSD (right) images of MIM processed samples; EBSD images showing the alpha-phase. All other phases (beta-phase, TiB-particles, pores) are displayed in black. In the case of MIM Ti64-B the regions of same orientation (same greyscale) appear to be smaller than in the case of MIM Ti64. Only few lamellar regions can be detected.

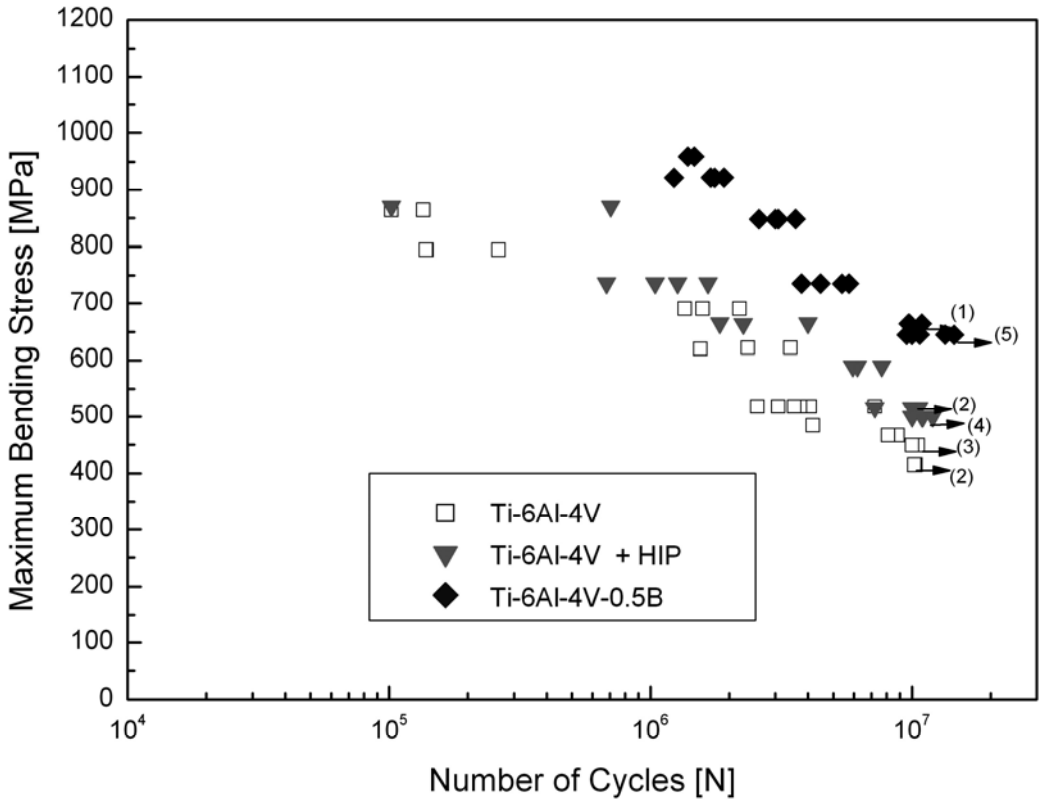

Fig. 5. Wöhler curves of three different samples tested: MIM-Ti64, MIM-Ti64+HIP and MIM-Ti64-B. The numbers in parentheses denote the amount of samples that survived at a specific stress level (run out). The finer microstructure of the boron added alloy effects a much larger increase in fatigue strength than the closing of the porosity by the HIP process. The endurance limit amounts to 640 MPa being well in the range of wrought Ti-6Al-4V material.

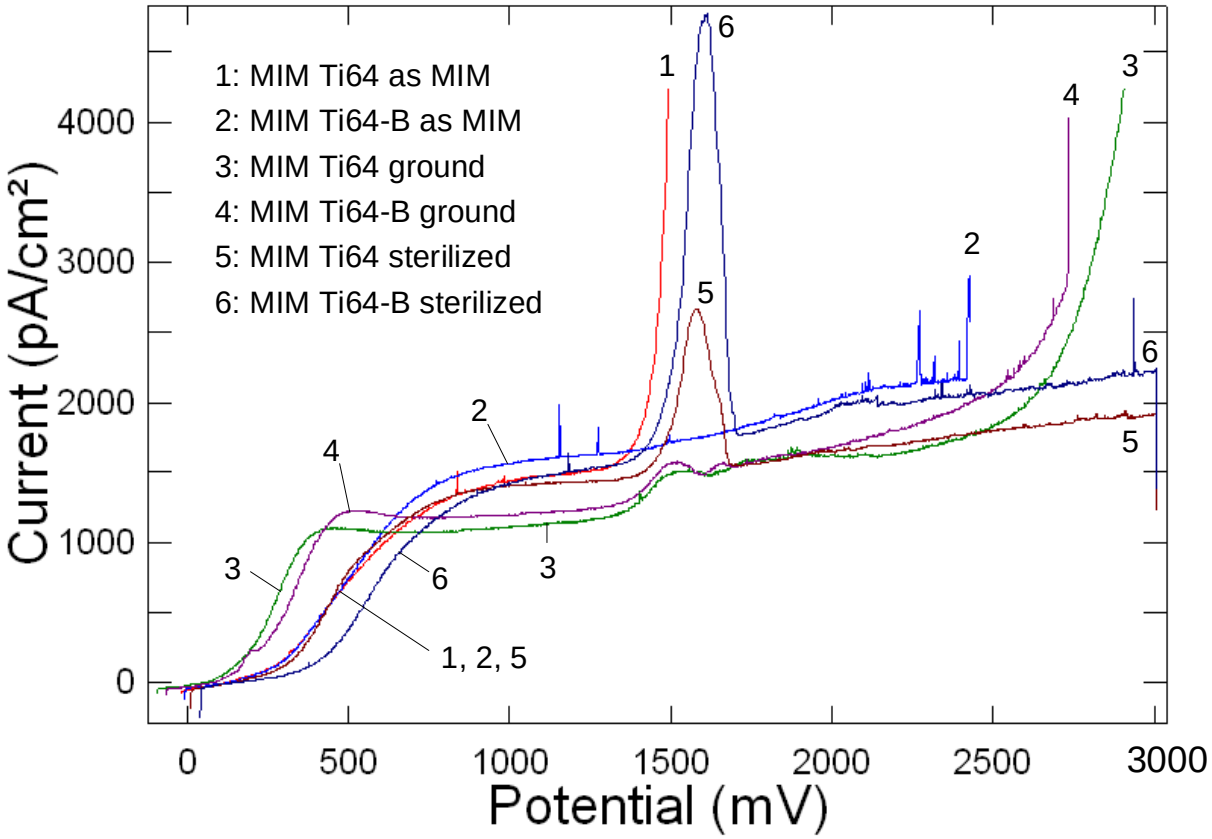

Fig. 6. Typical potential-current plots for the various alloy / surface condition combinations recorded by potentiodynamic polarisation in Ringer solution at room temperature.

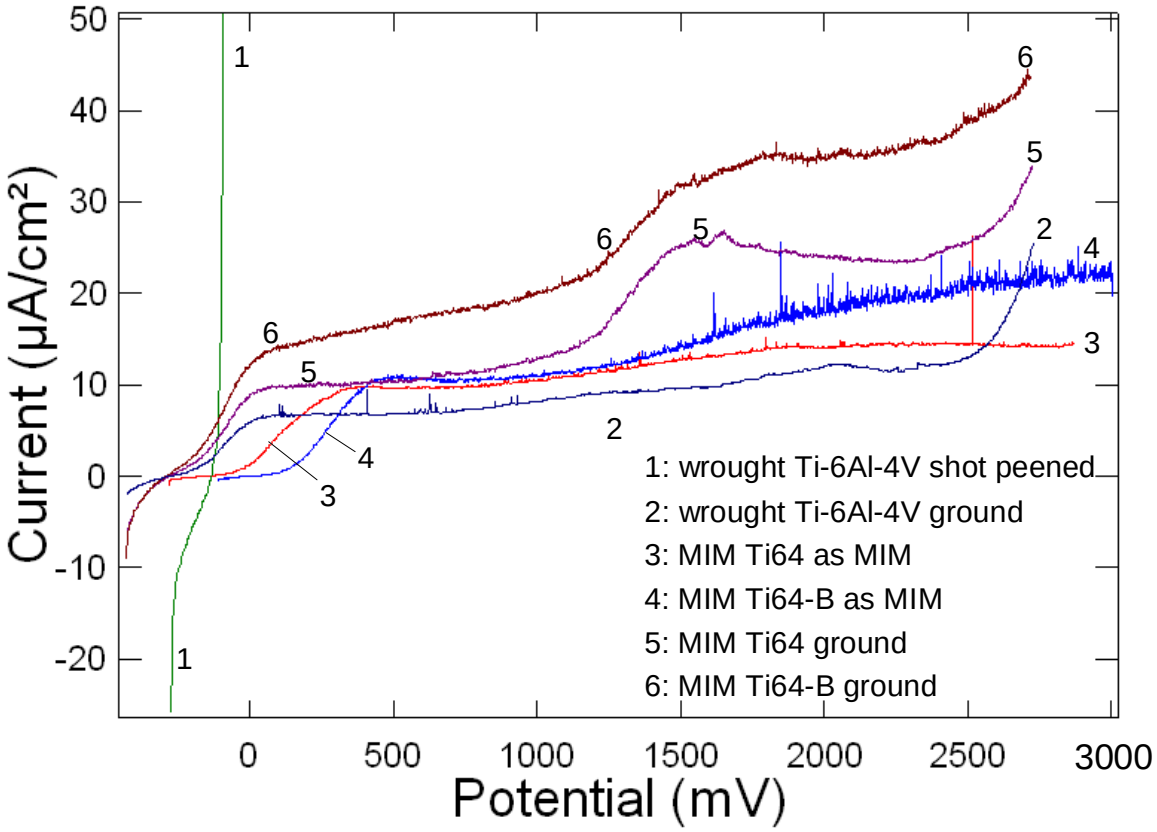

Fig. 7. Typical potential-current plots for the various alloy / surface condition combinations recorded by potentiodynamic polarisation in Ringer solution at 37.2°C.

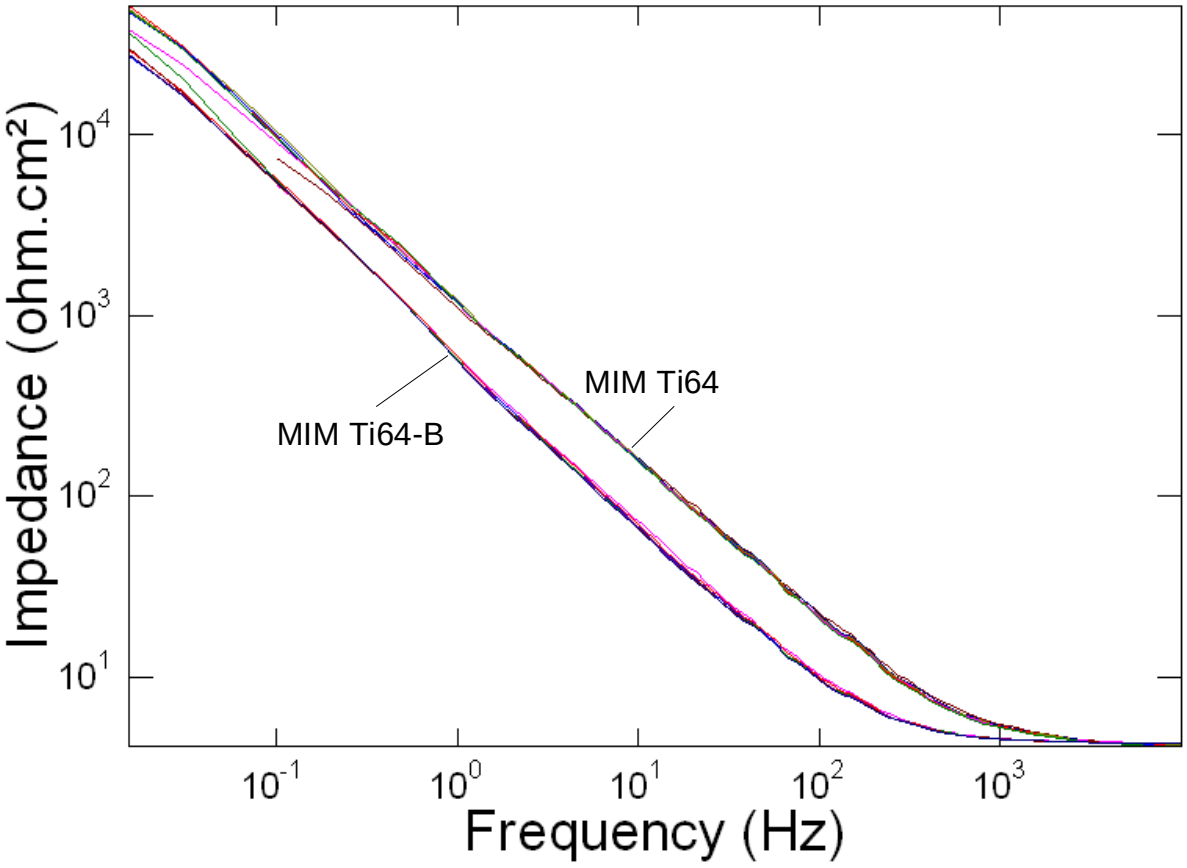

Fig. 8. Impedance plots for the two materials in the as MIM condition after various immersion times ranging from 2 to 170 hours in Ringer solution at 37.2°C

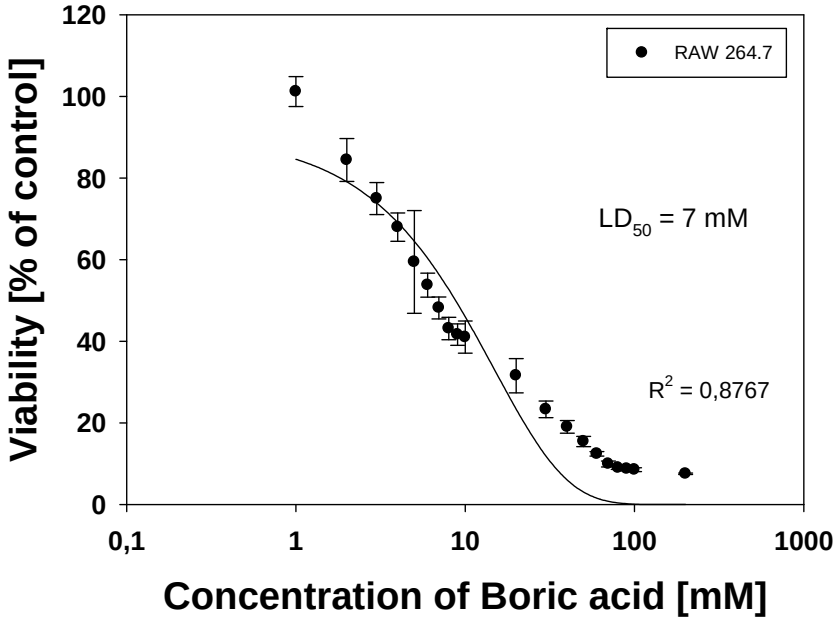

Fig. 9a. RAW 264.7 cell line

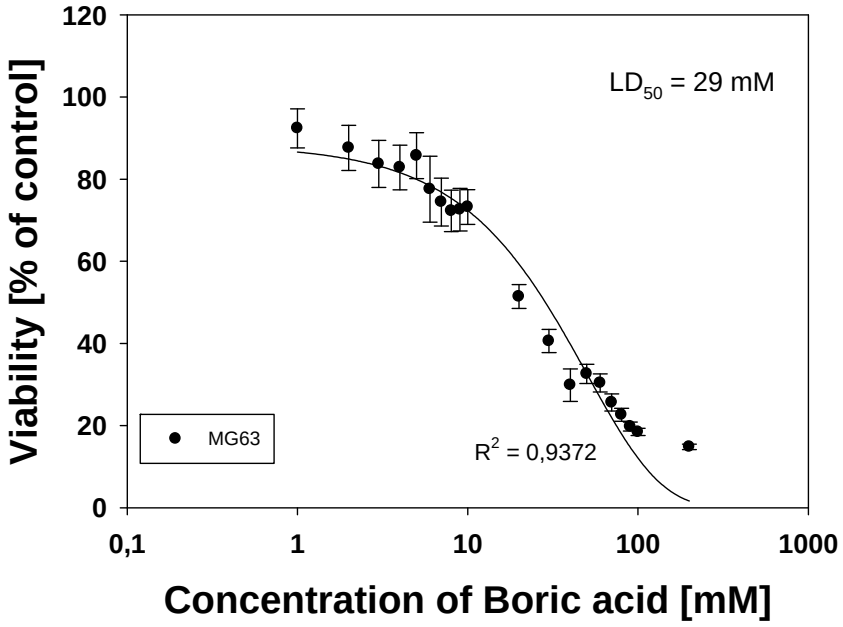

Fig. 9b. MG-63 cell line

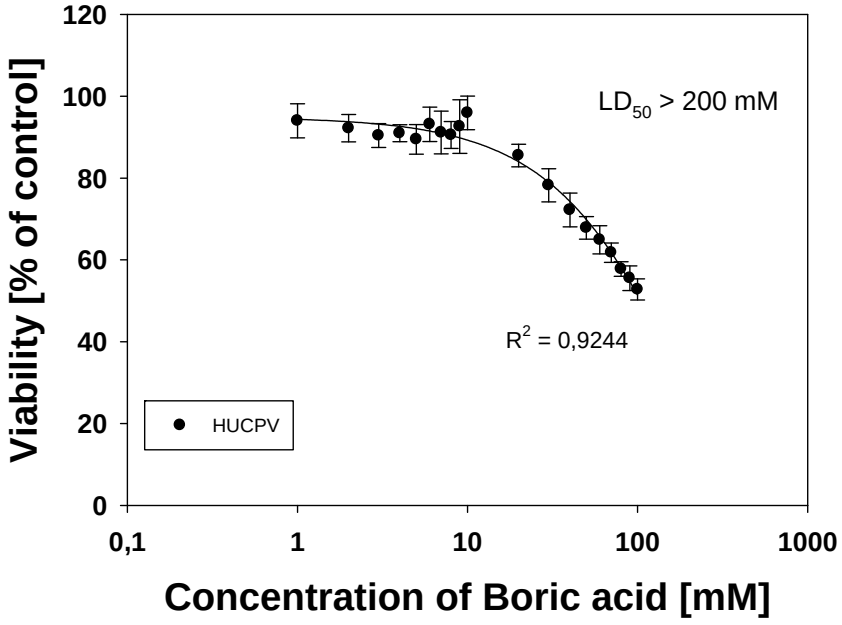

Fig. 9c HUCPV primary cells

Fig. 9. Viability data of different cell types exposed to increasing concentrations of boric acid. Given are the regression coefficients (R^2) and the half-lethal dose (LD_{50}). All regressions are highly significant ($p<0.001$).

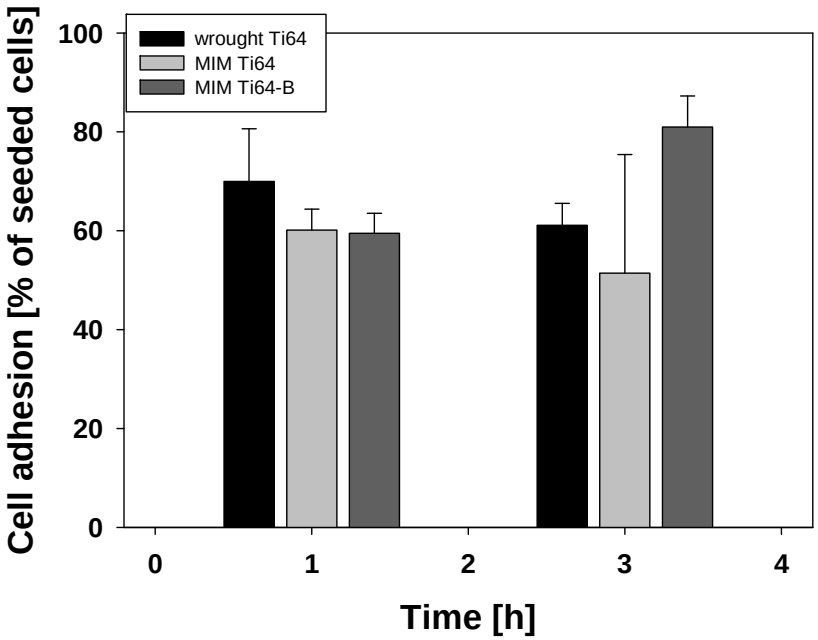

Fig. 10a. HUCPV primary cells

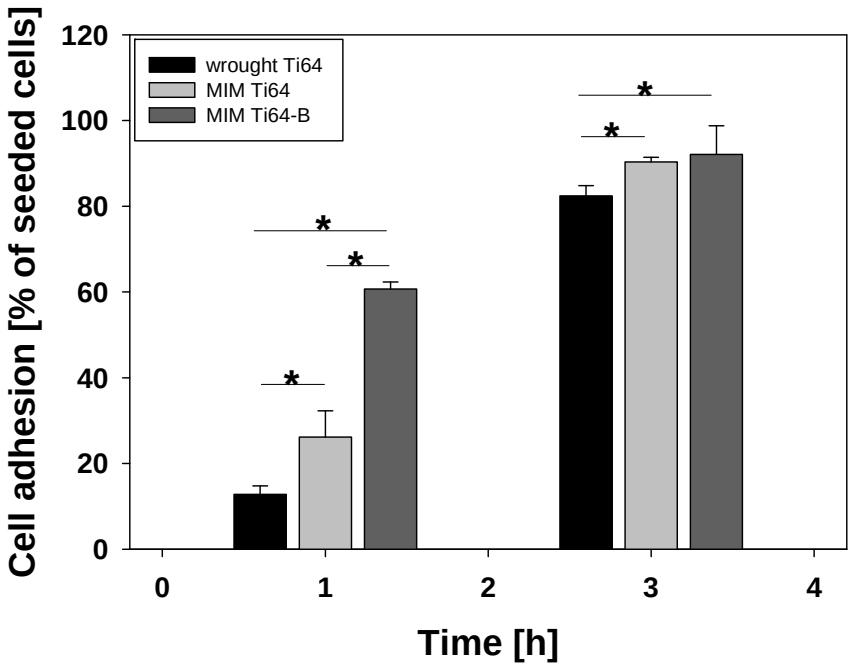

Fig. 10b. HBDC primary cells

*Fig 10. Cell adhesion after 1 and 3 hours of initially 100000 seeded cells of HUCPV (a) and HBDC (b determined by cell counting). Significant differences are depicted by asterisks (significance level * = p<0.05, one-way ANOVA)*

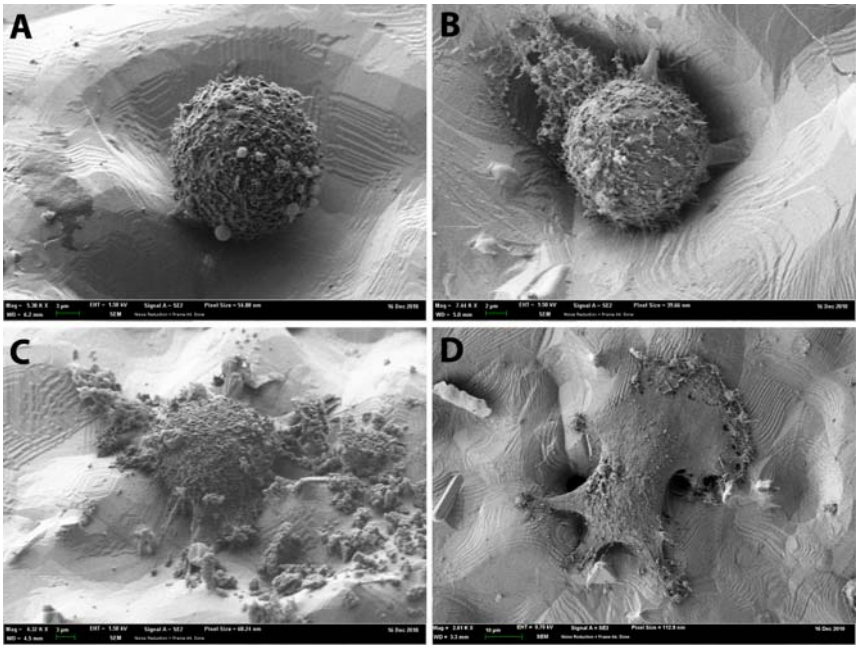

Fig 11. Human bone derived cells adhesion dynamic on MIM Ti64-B carrier shown by low voltage field emission SEM. First adhesion processes are visualised already after one hour (A and B). After 3 hours (C and D), adhesion of primary cells is complete, cells exhibiting a flattened morphology.

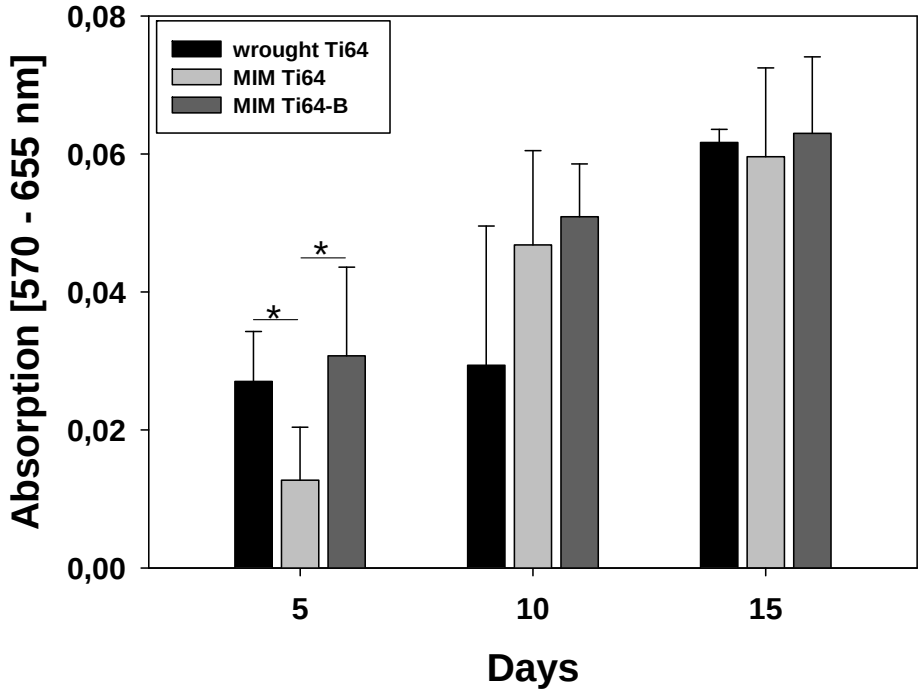

Fig 12. Cell proliferation determined by MTT of HUCPV after 5, 10 and 15 days. Significant differences are denominated by asterisks (= p<0.05, one-way ANOVA)*

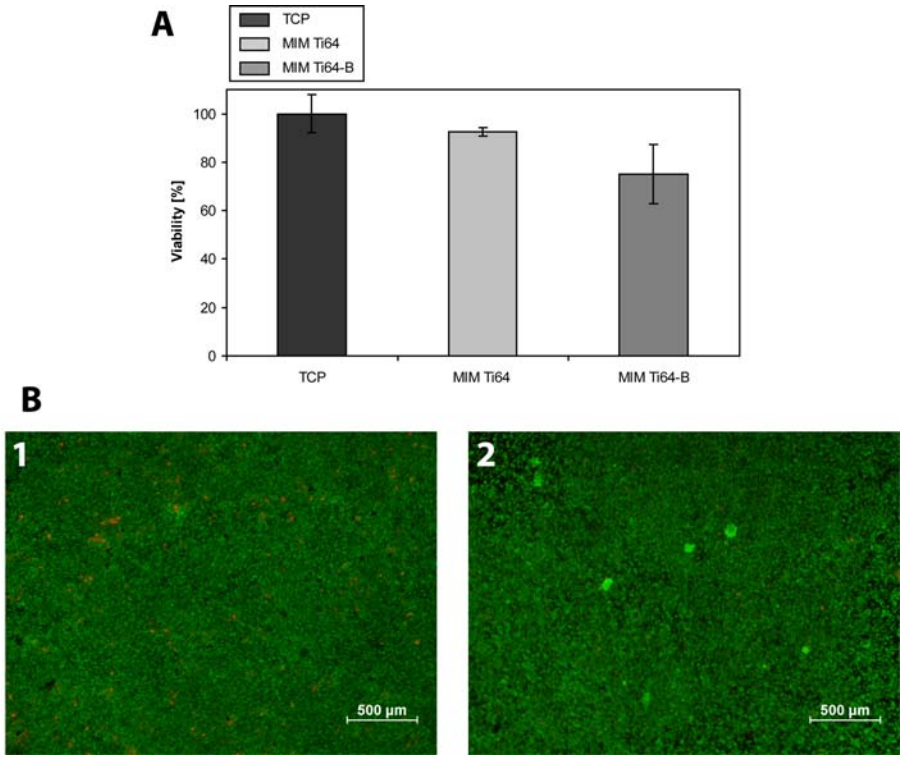

Fig 13. MG-63 cell viability determined after 3 days. A) Viability determined by measuring metabolically active cells (MTT colorimetric assay; B) LIVE/DEAD® cell viability staining on MIM Ti64 (1) and MIM Ti64-B (2); green cells are alive, red ones are dead. Note the higher amount of dead cells on MIM Ti64.

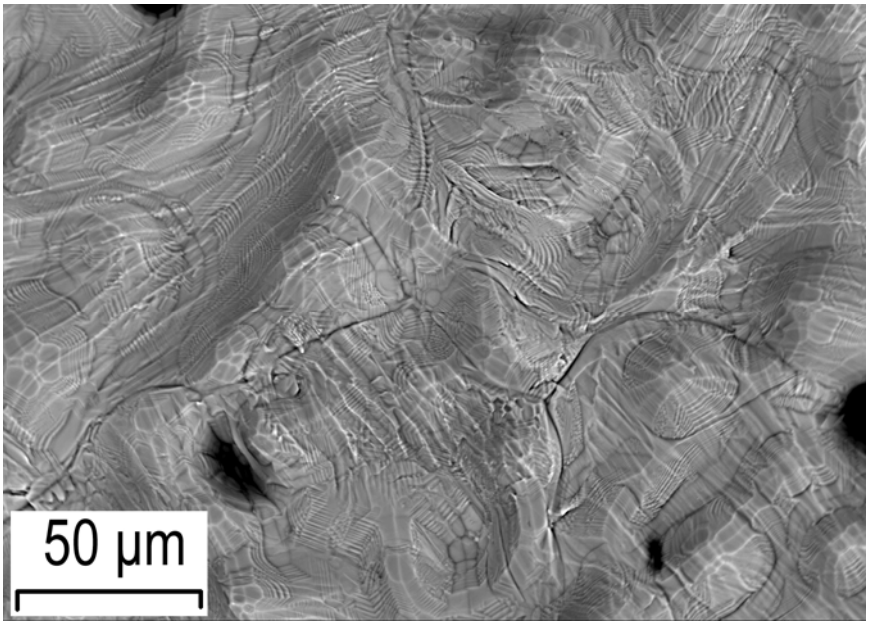

Fig. 14. SEM picture (BSE-mode) of the surface of a MIM Ti64 sample. The black regions are sintering pores, the white features represent β-phase, the gray ones a-phase. The black lines are grain boundaries.

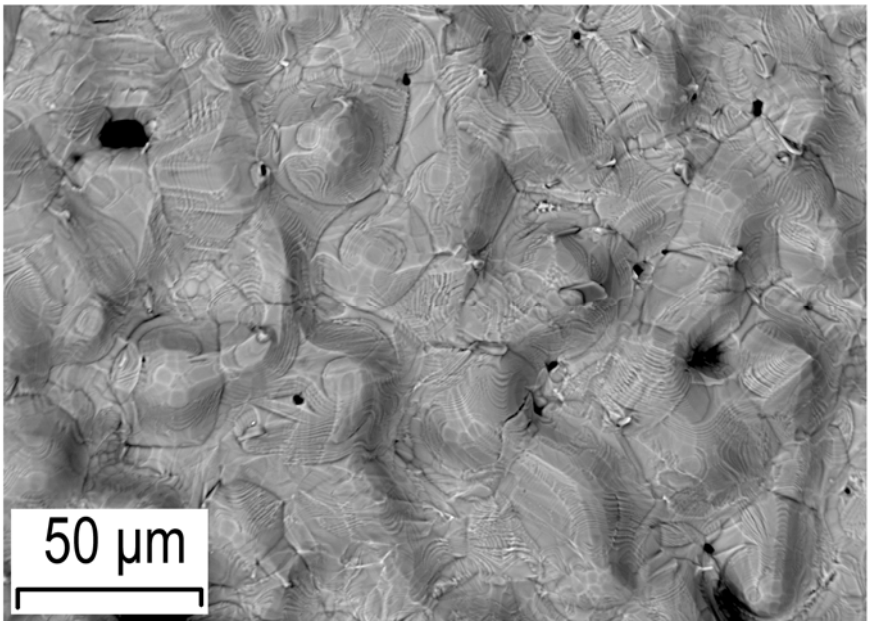

Fig 15. SEM picture (BSE-mode) of the surface of a MIM Ti64-B sample. In addition to MIM Ti64 in Figure 14, TiB particles are visible, partly penetrating the surface.

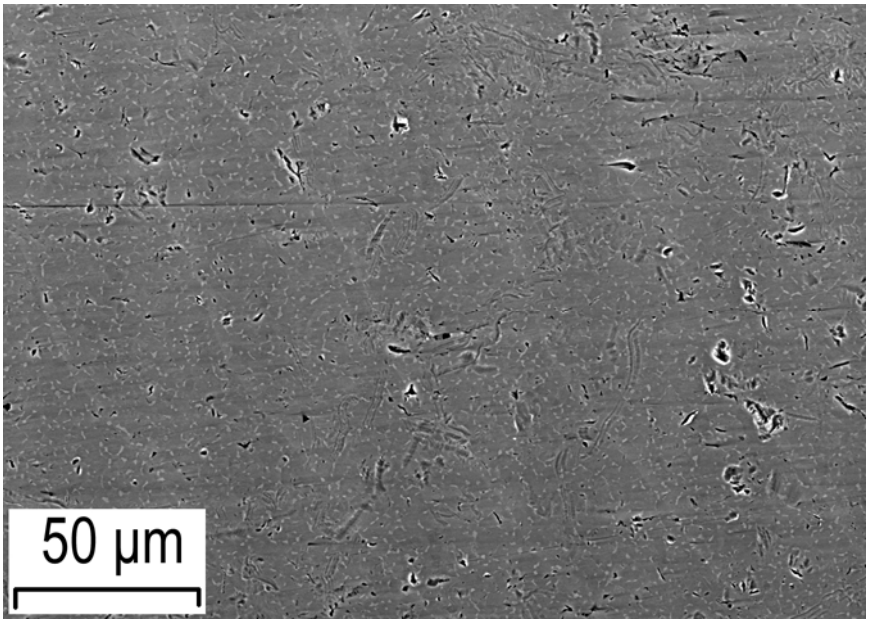

Fig 16. SEM picture (BSE-mode) of the surface of a wrought Ti64 sample. Larger structures are scratches from preparation.